HHS Public Access

Author manuscript

J Control Release. Author manuscript; available in PMC 2016 August 28.

Published in final edited form as:

J Control Release. 2015 August 28; 212: 30–40. doi:10.1016/j.jconrel.2015.06.007.

Effects of the Microbubble Shell Physicochemical Properties on Ultrasound-Mediated Drug Delivery to the Brain

Shih-Ying Wu[a], **Cherry C. Chen**[a], **Yao-Sheng Tung**[a], **Oluyemi O. Olumolade**[a], and **Elisa E. Konofagou**[a,b,*]

[a]Department of Biomedical Engineering, Columbia University, New York, NY 10027

[b]Department of Radiology, Columbia University, New York, NY 10032

Abstract

Lipid-shelled microbubbles have been used in ultrasound-mediated drug delivery. The physicochemical properties of the microbubble shell could affect the delivery efficiency since they determine the microbubble mechanical properties, circulation persistence, and dissolution behavior during cavitation. Therefore, the aim of this study was to investigate the shell effects on drug delivery efficiency in the brain via blood-brain barrier (BBB) opening *in vivo* using monodisperse microbubbles with different phospholipid shell components. The physicochemical properties of the monolayer were varied by using phospholipids with different hydrophobic chain lengths (C16, C18, and C24). The dependence on the molecular size and acoustic energy (both pressure and pulse length) were investigated. Our results showed that a relatively small increase in the microbubble shell rigidity resulted in a significant increase in the delivery of 40-kDa dextran, especially at higher pressures. Smaller (3 kDa) dextran did not show significant difference in the delivery amount, suggesting the observed shell effect was molecular size-dependent. In studying the impact of acoustic energy on the shell effects, it was found that they occurred most significantly at pressures causing microbubble destruction (450 kPa and 600 kPa); by increasing the pulse length to deliver the 40-kDa dextran, the difference between C16 and C18 disappeared while C24 still achieved the highest delivery efficiency. These indicated that the acoustic energy could be used to modulate the shell effects. The acoustic cavitation emission revealed the physical mechanisms associated with different shells. Overall, lipid-shelled microbubbles with long hydrophobic chain length could achieve high delivery efficiency for larger molecules especially with high acoustic energy. Our study, for the first time, offered evidence directly linking the microbubble monolayer shell with their efficacy for drug delivery *in vivo*.

Graphical Abstract

*Corresponding author.

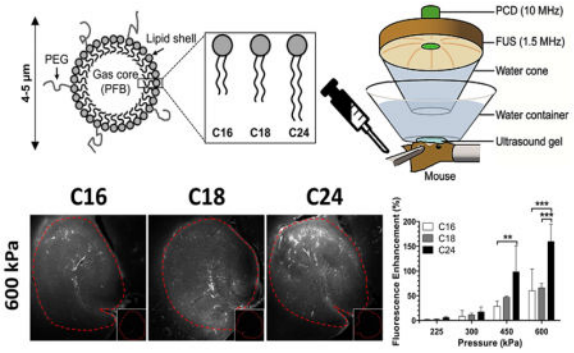

Keywords

drug delivery; ultrasound; microbubble; shell; blood-brain barrier; passive cavitation detection

1. Introduction

Microbubbles, gas-filled microspheres (1–10 μm) initially used merely as contrast agents for ultrasound imaging, have recently been shown critical in ultrasound-mediated therapeutic applications such as sonothrombolysis [1, 2], molecular delivery to the cell via sonoporation [3, 4] and/or endocytosis [5, 6], and to the brain parenchyma via blood-brain barrier (BBB) opening [7, 8] paracellularly or transcellularly. For molecular delivery purposes, although the biological mechanisms may vary, sonoporation and/or endocytosis and BBB opening share the same physical mechanism that cavitation increases the permeability of the cell membranes. In all the cases, the microbubble properties play important roles in determining the delivery efficiency. For example, larger microbubbles (4–5 μm in diameter) induce larger BBB opening and delivery efficiency than smaller microbubbles (1–2 μm in diameter) [9, 10]; soft-shelled (lipid or protein) microbubbles gave higher cell viability and transfection rate of gene delivery than hard-shelled (polymer) microbubbles [11].

Overall, the main goal of drug delivery is to achieve high efficiency without causing cell damage, and with the use of lipid-coated microbubbles it is achievable. In fact, with lipid-coated microbubbles the overall drug delivery efficiency could be influenced by changing the lipid hydrophobic chain length that modulates the overall physicochemical properties of the monolayer shell. Borden *et al.* have shown that increasing the lipid hydrophobic chain length increased the gas permeation resistance to the environment [12], decreased the acoustic dissolution rate while enhancing the lipid-shedding phenomenon during insonification [13]. Kwan *et al.* have reported that bubbles with longer lipid hydrophobic chains required longer re-stabilization following shell rupture, and longer to dissolve after the onset of collapse due to stronger attractive intermolecular forces [14, 15]. Longer acyl chains can also increase the lipid monolayer thickness [16] and microbubble mechanical properties such as in-plane rigidity [17], thereby modulating cavitation response and the shear stress applied on the cell membrane [18, 19]. Those results suggest that the physicochemical properties of the lipid-shelled microbubbles may play a role in affecting the drug delivery efficiency, but the exact effects remain to be discovered.

This study aimed at investigating the shell effect of lipid-coated microbubbles on the drug delivery efficiency *in vivo*. We hypothesize that increasing the lipid hydrophobic chain length would enhance the drug delivery efficiency after focused ultrasound (FUS)-induced BBB opening. The microbubbles used were coated with phosphatidylcholine (PC) lipids of various acyl chains (C16, C18, C24), and the phospholipid:lipopolymer ratio was fixed in order to isolate the effect of the PC acyl chain length. In addition, the diameter of the microbubble samples was kept constant at 4–5 μm in all experiments in order to exclude the influence of the microbubble size. Both molecular size (3 kDa and 40 kDa dextran been delivered), acoustic pressure (225–600 kPa), and pulse length (100 cycles and 1000 cycles) dependences were investigated in order to fully assess the microbubble shell effects on the drug delivery efficiency.

The different shelled microbubble dynamics *in vivo* were also captured during insonification using passive acoustic cavitation detection (PCD) in order to potentially uncover the physical mechanisms affecting the delivery efficiency such as micro-streaming and micro-jetting. The signal recorded by PCD is the acoustic emission from the cavitating bubbles, which represents the cavitation intensity with the signature of stable and/or inertial cavitation. We assume that the detected harmonics and ultraharmonics relate to stable cavitation (low and high amplitude bubble pulsation, or decaying oscillation) resulting in micro-streaming in a short or long period, and the detected broadband emission to inertial cavitation (violent bubble oscillation, bubble breakup or rebound) causing micro-jetting or shock wave emission, based on the bubble activities categorized by Leighton [20]. Both types of cavitation are thought to contribute to ultrasound-mediated drug delivery.

2. Materials and methods

2.1 Microbubble generation

All the lipids were purchased from Avanti Polar Lipids, Inc. (Alabaster, AL, USA), including 1,2-dipalmitoyl-sn-glycero-3-phosphocholine (DPPC or C16), 1,2-distearoyl-sn-glycero-3-phosphocholine (DSPC or C18), 1,2-dilignoceroyl-sn-glycero-3-phosphocholine (DLiPC or C24) and 1,2-distearoyl-sn-glycero-3phosphoethanolamine-N-[methoxy(polyethylene glycol)2000] (DSPE-PEG2000). The perfluorobutane gas (PFB, 99 wt% purity) used for microbubble generation was obtained from FluoroMed (Round Rock, TX, USA).

The lipid-coated microbubbles as shown in Fig. 1A were prepared at a 9:1 molar ratio of lipids and lipopolymers (DSPE-PEG2000). They were generated using the probe sonication method and size selected to 4–5 μm in diameter using differential centrifugation, as described elsewhere [21]. A Multisizer III particle counter (Beckman Coulter Inc., Opa Locka, FL, USA) with a 30-μm aperture was used to measure the microbubble size distribution (Fig. 1B–C) and concentration. The final size-isolated (4–5 μm) microbubble suspension was stored at 4 ºC till the time of injection. All the microbubble samples used for this study were freshly prepared within 24 h to ensure experimental consistency.

2.2 Animal and drug preparation

All animal experiments were conducted in accordance with procedures approved by the Columbia University Institutional Animal Care and Use Committee. A total of 123 male C57BL/6 mice (Harlan Laboratories, Indianapolis, IN, USA) weighing 20–25 g were used for this study. The animals were divided into five experimental groups depending on the ultrasound applied and the dextran molecule delivered during the FUS-induced BBB opening. The groups were further divided into 38 cohorts based on the experimental protocol as listed in Table 1. Before sonication, each mouse was anesthetized using 1–2% isoflurane-oxygen mixture (SurgiVet, Smiths Medical PM; Norwell, MA, USA) and its scalp fur was removed with an electric clipper and a depilatory cream. A modified 27G×½ butterfly catheter (Terumo Medical, Somerset, NJ, USA) was inserted into the tail vein for microbubble injection. The animal body temperature was maintained throughout the experiment using a heating pad.

Two dextran sizes were used separately as model drugs in this study. The 3-kDa and 40-kDa Texas Red-conjugated dextran with a Stoke-Einstein hydrodynamic diameter of 3 nm and 10 nm respectively were purchased from Life Technologies (Carlsbad, CA, USA) and dissolved to the same mass concentration (40 mg/mL) using sterile saline (Fisher Scientific, Pittsburgh, PA, USA). Therefore, the fluorescence enhancement was correlated to the mass of dextran being delivered rather than number of dextran molecules. All chemicals were used as purchased without further purification.

2.3 Ultrasound system for in vivo BBB opening

The experimental setup, as shown in Fig. 2A, was used as previously described [22]. A single-element, ring-shaped focused ultrasound (FUS) transducer (center frequency: 1.5 MHz, focal depth: 60 mm; Imasonic, Besancon, France) was driven by a function generator (33220A; Agilent Technologies, Palo Alto, CA, USA) through a 50 dB power amplifier (325LA; E&I, Rochester, NY, USA). A pulse-echo transducer (center frequency: 10 MHz, focal length: 60 mm; Olympus NDT, Waltham, MA, USA) confocally and coaxially aligned with the FUS transducer was used for both targeting and passive cavitation detection (PCD) purposes. During the targeting procedure, the pulse-echo transducer was driven by a pulser receiver (Model 5800; Parametrics-NDT, MA, USA) in transmit-and-receive mode; while for PCD during sonication, it was switched in receive-only mode with 20 dB of amplification. The signal was digitized in 50 MHz of sampling rate (CompuScope 1422, 14 bits; Gage Applied Technologies, Lachine, QC, Canada) and saved for offline processing.

The peak-rarefactional pressure profile used in the present study was estimated based on the calibration in degassed water with a bullet hydrophone (HGL-0400; Onda Corp., Sunnyvale, CA, USA), and the axial and lateral full-widths at half-maximum (FWHM) pressure of the focus were 10.6 mm and 1.3 mm, respectively. The pressure amplitudes were corrected to account for 18.1% attenuation through the murine skull as measured previously [8], and the derated peak-rarefactional pressure was reported in this study.

2.4 Experimental procedure

Pulsed FUS (excitation frequency: 1.5 MHz, pulsed length: 100 cycles (67 μs) or 1000 cycles (670 μs), pulse repetition frequency: 5 Hz, duration: 1 min) at acoustic pressures ranging between 225 and 600 kPa was applied transcranially to the targeted left hippocampus of the mouse brain while the right hippocampus served as the control without FUS. After the FUS transducer was aligned with the targeted region following the procedure described previously [8], the sonication procedure as illustrated in Fig. 2B was then followed. A 30 s of sonication was performed before microbubble injection as a baseline control for PCD. While at the same time the microbubble and dextran solution was prepared for the sonication with microbubble injection. The microbubble samples were freshly diluted to a final concentration of 8×10^8 bubbles/mL using sterile saline, and a 30 μL of the diluted microbubble suspension was co-administered with 50 μL dextran solution via bolus injection through the tail vein 5 s prior to the start of 1-min sonication. In addition, two sham cohorts without microbubble injection were injected with either the 3 kDa or the 40 kDa dextrans to serve as the basis for comparison of successful drug delivery in the fluorescence imaging analysis (see Section 2.5).

A 1-h period was allowed after sonication to enable the dextran to circulate throughout the vasculature and to diffuse into the brain parenchyma. At the end of the allotted time, the animal was sacrificed by transcardial perfusion using 30 mL phosphate buffer saline (PBS) for 5 min followed by 60 mL 4% paraformaldehyde for 8 min. The mouse brain was extracted from the skull, post-fixed in 4% paraformaldehyde overnight before sectioning for either fluorescence imaging or hematoxylin or eosin (H&E) staining in order to evaluate drug delivery efficiency and safety, respectively.

2.5 Fluorescence imaging and analysis

Followed by post-fixation process in Section 2.4, the brains for delivery efficiency analysis were cryoprotected (30% of sucrose for 48 hr) and then sectioned horizontally using a cryostat (Leica RM2255; Leica Microsystems Inc., Buffalo, IL, USA) into 60-μm slices covering the hippocampi. The 60-μm frozen sections were used to quantify the relative fluorescence enhancement representing the ratio of dextran (in mass) been delivered to the targeted hippocampus through BBB opening relative to the contralateral hippocampus (unsonicated), since the dextran mass was kept constant for injection.

The fluorescence intensity measurement was similarly performed following our previously reported procedure [22]. Both bright-field and epi-fluorescence images of the brain sections were captured using an Olympus DP25 and an Olympus DP30BW digital camera respectively mounted on an up-right Olympus BX61 microscope (Melville, NY, USA). Briefly, a section representing the ventral-dorsal midline, as determined by anatomical landmarks, was first selected, and four adjacent sections were then selected on either the ventral or the dorsal side of the midline. The left (sonicated) and the right (unsonicated control) hippocampus was manually outlined using MATLAB (Mathworks Inc., Natick, MA, USA), and the spatial average fluorescence intensity in the region of interest (ROI) was calculated using ImageJ (National Institutes of Health, Bethesda, MD, USA). The relative fluorescence enhancement was calculated by dividing the difference in fluorescence

intensity between the left and the right ROIs (removing the auto-fluorescence) by the fluorescence intensity in the right ROI (the spatial average of the right hippocampus and adding twice its standard deviation). For each brain, the reported fluorescence enhancement was thus approximately equal to the sum of the relative fluorescence intensity from all nine sections.

A successful dextran delivery for an individual brain was concluded if the fluorescence enhancement was higher by two standard deviations relative to the average of the corresponding sham cohort. The fluorescence enhancement value for each of the 36 experimental conditions was obtained by averaging all mice sonicated under the same acoustic exposure. 100% opening efficiency was concluded when all the mice evaluated in each cohort showed statistically significant dextran delivery.

2.6 Cavitation dose quantification for PCD

Three types of cavitation dose (SCD_h, stable cavitation dose using harmonics; SCD_u, stable cavitation dose using ultraharmonics; ICD, inertial cavitation dose) were quantified as described previously [22, 23]. First, each pulse of the PCD signal was calculated into the frequency spectrum in MATLAB (Mathworks Inc., Natick, MA, USA). Second, after taking the root mean square (rms) of the voltage spectral amplitude, the harmonic signal (n*f; n = 3, 4, 5, 6; f = 1.5 MHz; maximum amplitude within a bandwidth of 20 kHz around the harmonic frequency), ultraharmonic signal (n*f+0.5*f; n = 2, 3, 4, 5; f = 1.5 MHz; maximum amplitude within a bandwidth of 20 kHz around the ultraharmonic frequency), and the broadband signal in 3–9 MHz between them (applying a comb filter to suppress the harmonic and ultraharmonic signal with rejection bandwidths of 350 kHz and 100 kHz, respectively) were separately extracted. Third, the mean harmonic, ultraharmonic, and broadband signal were taken for each pulse and summed up over all pulses received during sonication to acquire SCD_h, SCD_u, and ICD, respectively. Lastly, the differential cavitation doses were computed by subtracting the normalized baseline cavitation doses (30s of sonication before microbubble injection). The cavitation doses reported in this study were the differential cavitation doses.

2.7 Histological evaluation

The histological examination for safety assessment of the entire hippocampi (both left and right) was performed via hematoxylin and eosin (H&E) staining, which can be used to identify damaged neurons (dark neurons showing shrunken and triangulated cell bodies) and red blood cell extravasations (hemorrhage) [24]. Only representative brain samples (n=6) from cohorts sonicated at the highest pressure level (600 kPa) were processed in order to assess potentially the most intense damage 1 hr after sonication. Followed by post-fixation process in Section 2.4, the brains in the safety assessment study were paraffin-embedded and then sectioned horizontally into 6-μm slices with 180-μm gaps covering the hippocampi. The bright field images of the stained slices were captured using the same microscope as mentioned previously. This histological examination was double-blinded, i.e., without knowledge of the microbubble type, the FUS exposure parameters, or the sonicated side.

2.8 Statistical analysis

The median diameters for the three microbubble types were compared using one-way ANOVA. The fluorescence enhancement and the cavitation doses for each group across all microbubble samples and pressure levels were compared using two-way ANOVA. The Bonferroni method was used to compare multiple pairs within the groups. The pair-wise p-values were considered statistically significant if they were lower than 0.05. In all the figures shown in this study, * represents $p < 0.05$, ** for $p < 0.01$, *** for $p < 0.001$, ns for $p > 0.05$, and the error bar for standard deviation. All statistical analyses were performed using GraphPad Prism (La Jolla, CA, USA).

3. Results

3.1 Microbubble generation and size-isolation

For each microbubble shell type, the probe sonication and differential centrifugation method produced an opaque milky microbubble suspension that was stable during the experimental timeframe. The mean, median and mode diameters of all microbubble samples, regardless of their shell lipid components, all fell within the range of 4 to 5 μm (Table 2). The representative number-weighted and volume-weighted size distributions of the microbubble samples as measured by the Coulter Multisizer III are showed in Fig. 1B–C. The size distributions and the diameters (mean, median and mode) among all microbubble suspensions used throughout the study were found to be statistically the same.

3.2 Drug delivery efficiency

Using fluorescently-labeled dextrans as model drug molecules, the delivery efficiency due to FUS-induced BBB opening could be quantified as the relative fluorescence enhancement in the sonicated hippocampus over the control. The two sham cohorts (Group 4 for 3-kDa dextran, Group 5 for 40-kDa dextran), for which no ultrasound was applied and no microbubbles were injected, did not show any change in fluorescence intensity between the two hemispheres (Suppl. Fig. 1). Quantified fluorescence enhancement results confirmed this observation as no detectable increase in fluorescence intensity between the two ROIs was acquired. For the rest of the 36 experimental conditions, the measured fluorescence enhancement was compared to their corresponding sham cohort in order to determine whether sufficient amount of dextran molecules were delivered to the targeted region. To study the shell effect on delivery efficiency with various drug molecule sizes, 3-kDa (Group 1) and 40-kDa (Group 2) dextrans were used as model drugs after FUS-induced BBB opening using 100-cycle (67 μs) pulses. To study the shell effect with various sonication pulse lengths, results of 100-cycle pulses (Group 2) and 1000-cycle pulses with 40-kDa dextrans (group 3) were compared.

Fig. 3 shows both the representative fluorescence images and the quantified enhancement results for Group 1 (3-kDa dextrans with 100-cycle pulses) after BBB opening. Due to the small molecular size, successful BBB opening was easily achieved at the lowest pressure level (225 kPa): 100% BBB opening efficiency was obtained for all mice regardless of the microbubble shell composition, with the exception of 1 mouse from the C24 microbubble/225 kPa cohort. The representative fluorescence images showed homogeneous

dextran diffusion within the sonicated locations with a fluorescence signal detected not only within or near large vessels, but also diffusely distributed across the entire hippocampi as the pressure increased (Fig. 3C–D, G–H, K–L). However, the difference was found to be statistically insignificant between shells (Fig. 3M).

Fig. 4 shows the representative fluorescence images for Group 2 (40-kDa dextrans with 100-cycle pulses). Under the same acoustic exposures regardless of the microbubble shell type, BBB opening was obtained in 100% of the mice sonicated using pressures at or above 300 kPa. However, at the lowest pressure level (225 kPa), successful BBB opening was not consistently achieved: 1 out of 3 mice sonicated using C16 microbubbles and 2 out of 3 mice sonicated using C24 microbubbles did not show significant fluorescence enhancement. C16 microbubbles mediated the smallest dextran diffusion within the targeted hippocampi at all pressure levels. Moreover, the detectable dextran signal was predominantly contained within the blood vessels even when some diffuse fluorescence enhancement within the targeted location was obtained as the pressure was increased above 300 kPa (Fig. 4C–D). On the other hand, significantly higher and more diffuse dextran distribution was induced using C18 and C24 microbubbles, especially at higher pressures (Fig. 4G–H, 4K–L). The quantified fluorescence analysis supported this finding (Fig. 4M). At 450 and 600 kPa, significantly higher 40-kDa dextran delivery was detected with both C18 and C24 microbubbles compared to C16 microbubbles. In addition, C24 microbubbles induced significantly more fluorescence enhancement at 600 kPa compared to C18 microbubbles.

Fig. 5 shows the representative fluorescence images for Group 3 (40-kDa dextrans with 1000-cycle pulses). 100% BBB opening efficiency was obtained in all animals regardless of the microbubble lipid chain length. Based on the fluorescence images (Fig. 5A–L), in stark contrast with the 100-cycle BBB opening findings, the longer acoustic pulses produced significantly more homogeneous diffusion of the 40-kDa dextran, especially with the longer C18 and C24 acyl chain lengths. Punctate clusters of dextran were still visible within the vessels at all pressure levels. The quantified fluorescence enhancement results showed significantly more dextran accumulation within the targeted hippocampi after BBB opening using C24 microbubbles at 450 and 600 kPa (Fig. 5M). On the other hand, no statistical difference in dextran delivery was detected between the C16 and C18 microbubbles across all pressure levels.

3.3 Acoustic cavitation emission

Three different types of cavitation dose (SCD_h, ICD, SCD_u) were separately quantified representing different bubble activities. Stable cavitation dose with harmonics (SCD_h) was for volumetric oscillation; inertial cavitation dose (ICD) identified drastic bubble oscillation and bubble collapse; stable cavitation dose with ultraharmonics (SCD_u) was thought to identify asymmetric oscillation and shell waves [23]. Fig. 6 shows the quantified acoustic cavitation dose during BBB opening using 100-cycle pulses (Fig. 6A–C) and 1000-cycle pulses (Fig. 6D–F). Using 100-cycle pulses, the SCD_h (Fig. 6A) for C18 and C24 was significantly higher than that of C16 at higher pressures, and the ICD and SCD_u for C24 was the highest (Fig. 6B–C). These results indicated that both C18 and C24 had stronger volumetric oscillation, and C24 had the strongest asymmetric oscillation potentially and

bubble collapse over the others, corresponding to the 40-kDa dextran delivery efficiency in Fig. 4. By increasing the pulse length to 1000 cycles (Fig. 6D–F), the cavitation difference among shells was compensated at lower pressures except at 600 kPa where the cavitation dose for C24 was still the highest, corresponding to the 40-kDa dextran delivery efficiency in Fig. 5.

3.4 Safety

Histological evaluation was performed in order to assess for potential tissue damage 1 hr after insonification. Fig. 7 shows the representative images obtained from all brain samples sonicated at the highest pressure (600 kPa). This pressure was selected since it represented the highest amount of exposed acoustic energy among all three groups. Examination at higher magnification did not reveal any discrete damage sites, such as clusters of dark neurons, small erythrocyte extravasations, hemorrhage or microvacuolations for brains sonicated with C16 microbubbles using either 100- or 1000-cycle pulses (Fig. 7A–B and 7G–H). Small clusters of dark neurons were identified from the representative brain that was sonicated with C18 microbubbles using 100-cycle pulses (Fig. 7C–D), while a few petechial hemorrhages were observed within the brain parenchyma sonicated with C18 microbubbles using 1000-cycle pulses (Fig. 7I–J). The most discernible abnormalities occurred in the C24 microbubble cohorts, for which a larger degree of microscopic perivascular hemorrhages was detected (Fig. 7E–F and 7K–L). However, the damage to the brain parenchyma was negligible. The severity of all observed tissue damages was concluded to be Category 1 to 2 with Category 0 representing no damage based on the criteria provided by Hynynen *et al.* [25].

3.5 Assessment of opening outcome using acoustic cavitation detection

The acoustic cavitation emission has been used to assess the drug delivery efficiency with acoustic responsive agents. In order to investigate whether the cavitation dose for different shelled microbubbles followed the same trend for assessing the BBB opening outcomes and drug delivery efficiency, both qualitative classification and quantitative analysis were performed as shown in Fig. 8. The total stable cavitation dose (SCD_{h+u}, sum of SCD_h and SCD_u) was adopted since it has been reported to correlate well with the drug delivery efficiency [22]. For the qualitative analysis (Fig. 8A), the SCD_{h+u} was separated into groups of no opening and opening based on the fluorescence results, and into groups of no damage and damage based on the histological findings. Despite the overlap, the SCD_{h+u} of the opening group was significantly higher than that of the no opening group for both 100-cycle and 1000-cycle pulses. The SCD_{h+u} of the no damage group was lower than that of the damage group. For quantitative analysis (Fig. 8B), the fluorescence enhancement was positively correlated with SCD_{h+u} for both 100-cycle and 1000-cycle pulses. The correlation curve of the SCD_{h+u} for different shelled microbubbles showed no difference.

4. Discussion

In this study, microbubbles with different phospholipid shell components were utilized to facilitate targeted drug delivery in the brain after FUS-induced BBB opening in mice. Based on the fluorescence analysis, our results clearly showed that increasing the hydrophobic

chain length of the phospholipid had a substantial effect on the larger 40-kDa dextran delivery (Fig. 4) while such effects were minimal for smaller molecules (3 kDa) (Fig. 3). Increasing the acoustic pulse length did not alter the shell effects using C24 microbubbles although the difference in 40-kDa dextran delivery amount became insignificant between the C16 and C18 microbubbles (Fig. 5). Histological examination showed increasing likelihood of minor tissue damage with the hydrophobic chain length (Fig. 7), further supporting our hypothesis that microbubble shell physicochemical properties directly affected their ability to mediate FUS-induced BBB opening. Quantified acoustic cavitation emission revealed possible physical mechanisms of the shell effects (Fig. 6), and was used to assess the opening outcome as well (Fig. 8). Our data suggests that, for a given acoustic exposure and microbubble size, the delivery efficiency is largely dictated by the microbubble shell. These results provided insight into how the shell composition might be used to increase the therapeutic efficacy in order to develop a more drug-specific FUS-induced BBB opening technology.

4.1 Microbubble shell physicochemical properties determining the drug delivery efficiency

Enhanced drug delivery with hydrophobic chain length in lipid-shelled microbubbles could be caused by the differences in (i) mechanical properties of the microbubbles, (ii) lipid buildup and shedding behavior, and (iii) microbubble persistence. Although the study was performed in FUS-induced BBB opening, the same concept may be applied to focused ultrasound and microbubble mediated drug delivery applications in general.

First, the difference in microbubble mechanical properties may affect the drug delivery efficiency by changing the force applied on the cell membrane through micro-streaming and micro-jetting during cavitation. For a lipid-shelled microbubble with longer hydrophobic chain length, the surface shear viscosity and surface yield shear were both higher, meaning that the shell became more rigid as the resistance to the shear deformation increased [17]. Besides, the microbubble stiffness may vary by adjusting the shell composition. As reported by Chen et al. using atomic force microscopy [26], the stiffness of C18 microbubbles in 4–5 μm was 15 mN/m, and adjustment of the shell composition could affect the overall stiffness [27]. Those differences could result in different shear stress on the cell membrane during cavitation as reported in simulation [18, 19].

Second, lipid buildup and shedding for microbubbles with longer hydrophobic chain length during cavitation could influence the process of drug delivery. Using high-speed microscopy, Borden *et al.* showed that microbubbles coated with longer hydrophobic chains had more cohesive shells and thus showed a higher probability of lipid buildup on their shells during sonication [13]. Therefore, it was possible that C18 and C24 microbubbles underwent a significant increase of the surface area through lipid buildup that has led to an increased contact area with the capillary endothelium during insonification. This induced higher shear stress along the vessel walls that may have led to more efficient drug delivery than with C16 microbubbles. In addition, the potentially increased shear stress could also explain the increased likelihood of minor petechial erythrocyte extravasation observed based on histological examination (Fig. 7). On the other hand, although microbubbles with shorter hydrophobic chains had lower delivery efficiency, their lipid shedding mechanism may

benefit the drug delivery applications using drug-loaded microbubbles [28–30]. C16 and C18 microbubbles with less cohesive shells could experience quasi-continuous to discrete phases of excessive lipid shedding and are capable of generating new micron-scale or smaller lipid vesicles [12, 13]. This mechanism has been used for multimodality imaging by converting microbubbles to nanoparticles after applying ultrasound [31]. Those small vesicles if carrying drugs could potentially be delivered to the cell as drug-loaded nanobubbles [32, 33].

Third, higher persistence for microbubbles with longer hydrophobic chain lengths during cavitation and circulation *in vivo* may enhance the drug delivery efficiency as well. It was reported that longer-acyl-chain (C18 or C24) microbubbles had higher resistance to natural gas permeation [12], acoustic dissolution and monolayer collapse due to the increased intermolecular cohesiveness of the shell [13–15]. Therefore, it is plausible to assume that the increased monolayer stability for microbubbles coated with longer acyl chains could prolong the *in vivo* microbubble persistence during circulation and insonification, which could ultimately lead to increased dextran delivery. Even though Garg *et al.* showed that a hydrophobic mismatch could reduce the circulation time of DLiPC:DSPE-PEG5000 microbubbles [34], we did not observe any significant decrease in persistence of our C24 microbubbles based on the cavitation signal acquired during sonication when compared to C16 or C18 microbubbles. We attribute the discrepancies between these two studies to the differences in the experimental designs, including microbubble dosage, sonication and detection duration, signal detection methods including targeting organs (brain through the skull vs. kidney) as well as acoustic pulse sequences (different mechanical indexes, pulse lengths, pulse repetition frequencies).

4.2 Shell properties determined the delivery efficiency of large molecules

The observed microbubble shell effect appeared to be molecular size-dependent. Based on fluorescence analysis, there was no significantly different delivery amount detected for 3 kDa dextran among the various microbubble shells at each pressure (Fig. 3), while a difference was obtained at 40 kDa dextran delivery at pressures causing microbubble destruction or inertial cavitation (450 kPa and 600 kPa) (Fig. 4 and Fig. 5). This suggests that the microbubble shell effects were only dominant if the delivered agent has a size above that threshold, since a large amount of small molecules could easily permeate across the BBB in a short time until reaching saturation. Moreover, it also indicates that microbubbles of longer hydrophobic chain (C24) could be used to enhance the delivery efficiency of large molecules. This is promising since delivering large molecules has been shown challenging after BBB opening [35, 36].

4.3 Acoustic energy (by varying pressure and pulse length) modulated the shell effects

The shell effects occurred most significantly at pressures causing microbubble destruction or inertial cavitation (450 kPa and 600 kPa) (Fig. 4 and Fig. 5) may be due to more lipid buildup that cause higher shear stress generated on the cell membrane. The lipid buildup behavior during insonification may be dominant at intermediate or high pressures since the bubble oscillation amplitude is higher. This is consistent with the previous study using a

pressure of 400 kPa or higher to observe lipid buildup in the microbubble shell with a high-speed camera [13].

Increasing the pulse length did not alter the general trend of the microbubble shell effect although the difference in fluorescence enhancement between C16 and C18 microbubbles became statistically insignificant (Fig. 5). As shown in previous studies, the drug delivery efficiency increased with the pulse length until it reached to a plateau [37]. This principle could also be applied to microbubbles of various hydrophobic chain lengths. The significantly longer pulse length effect for C24 microbubbles may be due to the bubble's higher persistence to dissolution and collapse *in vivo* as the delivery efficiency remained significantly higher than others. Our data suggests that the increased pulse length could be used to compensate for the microbubble shell effects when the hydrophobic chain lengths were close (e.g., C16 and C18). Furthermore, using microbubbles of longer hydrophobic chain length in combination with longer pulse length could maximize the delivery efficiency for large molecules.

Overall, it is possible that the shell effects on drug delivery efficiency were dependent on the interactions between the acoustic energy and the drug properties, such as molecular size, molecular structure (linear vs. globular), and hydrophobicity (water-soluble vs. lipid-soluble). In the future, additional systematic and parametric studies could be performed to determine the optimal ultrasound and microbubble combination that achieves optimal delivery dose for various drugs without compromising safety.

4.4 Acoustic cavitation detection revealed the microbubble shell effects

Passive cavitation detection (PCD) revealed the possible physical mechanisms behind the *in vivo* microbubble shell effects. PCD offers an indirect way to record the microbubble dynamics *in vivo* both noninvasively and transcranially, in which other methods such as high-speed camera or B-mode imaging could hardly achieve. PCD records cavitation signatures including stable and inertial cavitation causing micro-streaming and micro-jetting [20]. The quantified SCD_h could be related to microbubble circulation persistence which is usually measured with B-mode imaging, ICD to shock wave or force generated by microbubble collapse, and both SCD_h and SCD_u (SCD_{h+u}) to the shear stress applied on the cell membrane, which were thus used to assess the BBB opening outcome (Fig. 8). In these scenarios, the circulation persistence and the strength from microbubble collapse for C24 may surpass other microbubbles, thereby delivering more 40kDa dextrans to the brain.

4.5 The most intense tissue damage was minor and recoverable

Histological evaluation was performed for cohorts using the highest pressure (600 kPa) and sacrificed 1 hr after sonication in order to assess the most intense tissue damage within the first hour. Although it showed an increased likelihood of petechial hemorrhage with increasing hydrophobic chain length as well as one case with dark neurons using C18 microbubbles, those damage were minor (Categories 1–2) which usually came without ischemic neurons or cell apoptosis [25]. Further, both dark neurons [24] and red blood cell (RBC) extravasations [38] were recoverable.

More intensive toxicological assessment of ultrasound-mediated BBB opening was performed in non-human primates, paving the way to clinical applications. First, the BBB opening was reversible, which was reported to recover within four days after an opening without detected hemorrhage or edema [39]. Second, short-term safety evaluation using MRI within 48 hr after sonication showed that repetitive BBB opening without detected hemorrhage or edema was achievable [39, 40]. Third, long-term safety evaluation using histological staining after consecutive sonication over several months showed only a small degree of RBC extravasations (Categories 1–2) with no evidence of other tissue or cell damage such as demyelination and apoptotic bodies [40]. Forth, no functional deficits such as acuity was found in behavioral tests from hours to months after repetitively inducing BBB opening in visual area [40].

5. Conclusion

The effects of the microbubble shell physicochemical properties on drug delivery efficiency using ultrasound have been characterized using microbubbles of three phospholipids with increasing hydrophobic chain lengths (C16, C18, C24) for drug delivery to the brain through BBB opening. The entire process was monitored using passive acoustic cavitation detection (PCD) in order to shed light on the physical mechanisms behind the shell effects. The dependence on both the molecular size and acoustic energy (by varying pressure and pulse length) were studied. We showed that relatively small changes in lipid hydrophobic chain length resulted in a significant increase for large (40 kDa) but not for small (3 kDa) dextran delivery, and the acoustic energy modulated the shell effects on the delivery efficiency. The C24 microbubble was deemed to be the most efficient for large-molecule delivery. Acoustic cavitation detection revealed possible mechanisms with different shells, and the findings showed a good correlation between the delivery efficiency and tissue damage for different shelled microbubbles.

Supplementary Material

Refer to Web version on PubMed Central for supplementary material.

Acknowledgments

This research was supported in part by the National Institutes of Health grants R01 EB009041 and R01 AG038961. The authors would like to thank Wenlan Zheng and Hong Chen at Columbia University for assisting with the manuscript.

References

1. Molina CA, Barreto AD, Tsivgoulis G, Sierzenski P, Malkoff MD, Rubiera M, Gonzales N, Mikulik R, Pate G, Ostrem J, Singleton W, Manvelian G, Unger EC, Grotta JC, Schellinger PD, Alexandrov AV. Transcranial ultrasound in clinical sonothrombolysis (TUCSON) trial. Ann Neurol. 2009; 66:28–38. [PubMed: 19670432]
2. Culp WC, Flores R, Brown AT, Lowery JD, Roberson PK, Hennings LJ, Woods SD, Hatton JH, Culp BC, Skinner RD, Borrelli MJ. Successful microbubble sonothrombolysis without tissue-type plasminogen activator in a rabbit model of acute ischemic stroke. Stroke. 2011; 42:2280–2285. [PubMed: 21700942]

3. Mehier-Humbert S, Bettinger T, Yan F, Guy RH. Plasma membrane poration induced by ultrasound exposure: implication for drug delivery. J Control Release. 2005; 104:213–222. [PubMed: 15866347]

4. van Wamel A, Kooiman K, Harteveld M, Emmer M, ten Cate FJ, Versluis M, de Jong N. Vibrating microbubbles poking individual cells: drug transfer into cells via sonoporation. J Control Release. 2006; 112:149–155. [PubMed: 16556469]

5. Meijering BDM, Juffermans LJM, van Wamel A, Henning RH, Zuhorn IS, Emmer M, Versteilen AMG, Paulus WJ, van Gilst WH, Kooiman K, de Jong N, Musters RJP, Deelman LE, Kamp O. Ultrasound and Microbubble-Targeted Delivery of Macromolecules Is Regulated by Induction of Endocytosis and Pore Formation. Circulation Research. 2009; 104:679–U226. [PubMed: 19168443]

6. De Cock I, Zagato E, Braeckmans K, Luan Y, de Jong N, De Smedt SC, Lentacker I. Ultrasound and microbubble mediated drug delivery: Acoustic pressure as determinant for uptake via membrane pores or endocytosis. J Control Release. 2015; 197:20–28. [PubMed: 25449801]

7. Hynynen K, McDannold N, Vykhodtseva N, Jolesz FA. Noninvasive MR imaging-guided focal opening of the blood-brain barrier in rabbits. Radiology. 2001; 220:640–646. [PubMed: 11526261]

8. Choi JJ, Pernot M, Small SA, Konofagou EE. Noninvasive, transcranial and localized opening of the blood-brain barrier using focused ultrasound in mice. Ultrasound Med Biol. 2007; 33:95–104. [PubMed: 17189051]

9. Choi JJ, Feshitan JA, Baseri B, Wang S, Tung YS, Borden MA, Konofagou EE. Microbubble-size dependence of focused ultrasound-induced blood-brain barrier opening in mice in vivo. IEEE Trans Biomed Eng. 2010; 57:145–154. [PubMed: 19846365]

10. Tung YS, Vlachos F, Feshitan JA, Borden MA, Konofagou EE. The mechanism of interaction between focused ultrasound and microbubbles in blood-brain barrier opening in mice. J Acoust Soc Am. 2011; 130:3059–3067. [PubMed: 22087933]

11. Mehier-Humbert S, Yan F, Frinking P, Schneider M, Guy RH, Bettinger T. Ultrasound-mediated gene delivery: influence of contrast agent on transfection. Bioconjug Chem. 2007; 18:652–662. [PubMed: 17419583]

12. Borden MA, Longo ML. Dissolution behavior of lipid monolayer-coated, air-filled microbubbles: effect of lipid hydrophobic chain length. Langmuir. 2002; 18:9225–9233.

13. Borden MA, Kruse DE, Caskey CF, Zhao S, Dayton PA, Ferrara KW. Influence of lipid shell physicochemical properties on ultrasound-induced microbubble destruction. IEEE Trans Ultrason Ferroelectr Freq Control. 2005; 52:1992–2002. [PubMed: 16422411]

14. Kwan JJ, Borden MA. Lipid monolayer dilatational mechanics during microbubble gas exchange. Soft Matter. 2012; 8:4756–4766.

15. Kwan JJ, Borden MA. Lipid monolayer collapse and microbubble stability. Adv Colloid Interface Sci. 2012; 183–184:82–99.

16. Lewis BA, Engelman DM. Lipid bilayer thickness varies linearly with acyl chain length in fluid phosphatidylcholine vesicles. J Mol Biol. 1983; 166:211–217. [PubMed: 6854644]

17. Kim DH, Costello MJ, Duncan PB, Needham D. Mechanical properties and microstructure of polycrystalline phospholipid monolayer shells: Novel solid microparticles. Langmuir. 2003; 19:8455–8466.

18. Wu J. Theoretical study on shear stress generated by microstreaming surrounding contrast agents attached to living cells. Ultrasound Med Biol. 2002; 28:125–129. [PubMed: 11879959]

19. Doinikov AA, Bouakaz A. Theoretical investigation of shear stress generated by a contrast microbubble on the cell membrane as a mechanism for sonoporation. J Acoust Soc Am. 2010; 128:11–19. [PubMed: 20649196]

20. Leighton, TG. The Acoustic Bubble. 1994.

21. Feshitan JA, Chen CC, Kwan JJ, Borden MA. Microbubble size isolation by differential centrifugation. J Colloid Interface Sci. 2009; 329:316–324. [PubMed: 18950786]

22. Chen CC, Sheeran PS, Wu SY, Olumolade OO, Dayton PA, Konofagou EE. Targeted drug delivery with focused ultrasound-induced blood-brain barrier opening using acoustically-activated nanodroplets. J Control Release. 2013; 172:795–804. [PubMed: 24096019]

23. Wu SY, Tung YS, Marquet F, Downs M, Sanchez C, Chen C, Ferrera V, Konofagou E. Transcranial cavitation detection in primates during blood-brain barrier opening--a performance

assessment study. IEEE Trans Ultrason Ferroelectr Freq Control. 2014; 61:966–978. [PubMed: 24859660]

24. Baseri B, Choi JJ, Tung YS, Konofagou EE. Multi-Modality Safety Assessment of Blood-Brain Barrier Opening Using Focused Ultrasound and Definity Microbubbles: A Short-Term Study. Ultrasound Med Biol. 2010; 36:1445–1459. [PubMed: 20800172]
25. Hynynen K, McDannold N, Martin H, Jolesz FA, Vykhodtseva N. The threshold for brain damage in rabbits induced by bursts of ultrasound in the presence of an ultrasound contrast agent (Optison). Ultrasound Med Biol. 2003; 29:473–481. [PubMed: 12706199]
26. Chen CC, Wu SY, Finan JD, Morrison B, Konofagou E. An experimental study on the stiffness of size-isolated microbubbles using atomic force microscopy. IEEE Trans Ultrason Ferroelectr Freq Control. 2013; 60:524–534. [PubMed: 23475918]
27. Abou-Saleh RH, Swain M, Evans SD, Thomson NH. Poly(ethylene glycol) lipid-shelled microbubbles: abundance, stability, and mechanical properties. Langmuir. 2014; 30:5557–5563. [PubMed: 24758714]
28. Tinkov S, Coester C, Serba S, Geis NA, Katus HA, Winter G, Bekeredjian R. New doxorubicin-loaded phospholipid microbubbles for targeted tumor therapy: in-vivo characterization. J Control Release. 2010; 148:368–372. [PubMed: 20868711]
29. Sirsi SR, Hernandez SL, Zielinski L, Blomback H, Koubaa A, Synder M, Homma S, Kandel JJ, Yamashiro DJ, Borden MA. Polyplex-microbubble hybrids for ultrasound-guided plasmid DNA delivery to solid tumors. J Control Release. 2012; 157:224–234. [PubMed: 21945680]
30. Fan CH, Ting CY, Lin HJ, Wang CH, Liu HL, Yen TC, Yeh CK. SPIO-conjugated, doxorubicin-loaded microbubbles for concurrent MRI and focused-ultrasound enhanced brain-tumor drug delivery. Biomaterials. 2013; 34:3706–3715. [PubMed: 23433776]
31. Huynh E, Leung BY, Helfield BL, Shakiba M, Gandier JA, Jin CS, Master ER, Wilson BC, Goertz DE, Zheng G. In situ conversion of porphyrin microbubbles to nanoparticles for multimodality imaging. Nat Nanotechnol. 2015
32. Wang Y, Li X, Zhou Y, Huang P, Xu Y. Preparation of nanobubbles for ultrasound imaging and intracelluar drug delivery. Int J Pharm. 2010; 384:148–153. [PubMed: 19781609]
33. Hwang TL, Lin YK, Chi CH, Huang TH, Fang JY. Development and evaluation of perfluorocarbon nanobubbles for apomorphine delivery. J Pharm Sci. 2009; 98:3735–3747. [PubMed: 19156914]
34. Garg S, Thomas AA, Borden MA. The effect of lipid monolayer in-plane rigidity on in vivo microbubble circulation persistence. Biomaterials. 2013; 34:6862–6870. [PubMed: 23787108]
35. Choi JJ, Wang S, Tung YS, Morrison B 3rd, Konofagou EE. Molecules of various pharmacologically-relevant sizes can cross the ultrasound-induced blood-brain barrier opening in vivo. Ultrasound Med Biol. 2010; 36:58–67. [PubMed: 19900750]
36. Chen H, Konofagou EE. The size of blood-brain barrier opening induced by focused ultrasound is dictated by the acoustic pressure. J Cereb Blood Flow Metab. 2014; 34:1197–1204. [PubMed: 24780905]
37. Choi JJ, Selert K, Gao Z, Samiotaki G, Baseri B, Konofagou EE. Noninvasive and localized blood-brain barrier disruption using focused ultrasound can be achieved at short pulse lengths and low pulse repetition frequencies. J Cereb Blood Flow Metab. 2010
38. McDannold N, Vykhodtseva N, Raymond S, Jolesz FA, Hynynen K. MRI-guided targeted blood-brain barrier disruption with focused ultrasound: histological findings in rabbits. Ultrasound in medicine & biology. 2005; 31:1527–1537. [PubMed: 16286030]
39. Marquet F, Teichert T, Wu SY, Tung YS, Downs M, Wang S, Chen CC, Ferrera VP, Konofagou EE. Real-time transcranial monitoring of safe blood-brain barrier opening in non-human primates. PLoS ONE. 2014; 9:e84310. [PubMed: 24505248]
40. McDannold N, Arvanitis CD, Vykhodtseva N, Livingstone MS. Temporary disruption of the blood-brain barrier by use of ultrasound and microbubbles: safety and efficacy evaluation in rhesus macaques. Cancer research. 2012; 72:3652–3663. [PubMed: 22552291]

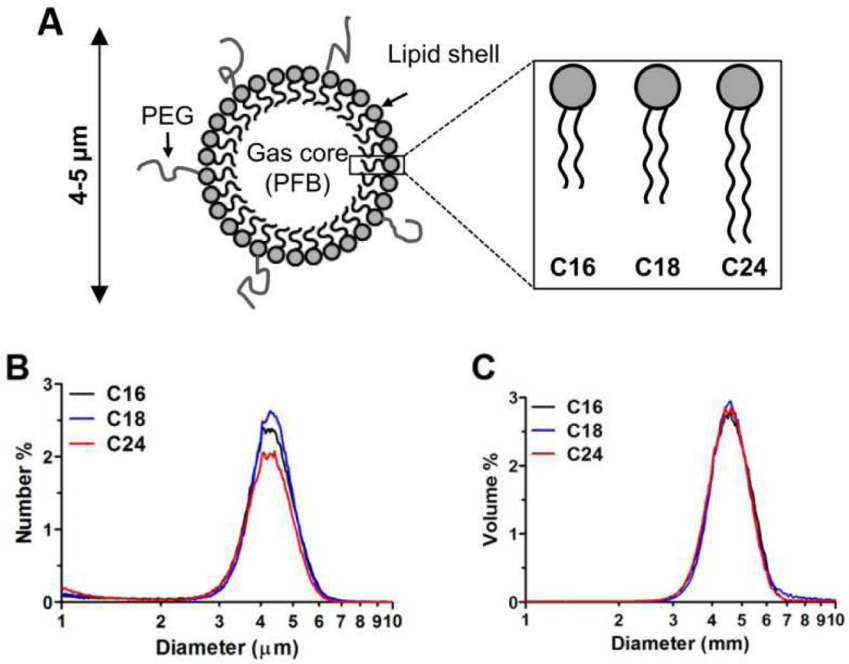

Fig. 1.

Schematic of the lipid-shelled microbubble used in this study (A) and their representative size distribution in number (B) and volume (C). Three different lipid acyl chain lengths (C16, C18, C24) were used to generate microbubbles of different physicochemical properties, while the emulsifier (DSPE-PEG2000), the molar ratio between the main lipid and the emulsifier (9:1), the gas core (PFB), and the size of the microbubbles (4–5 μm) were kept the same in order to focus on the effects of lipid hydrophobic chain length. The size of the different-shelled microbubbles was statistically the same (Table 2). All microbubble suspensions were diluted to the same concentration (8×10^8 particle/mL) immediately prior to injection.

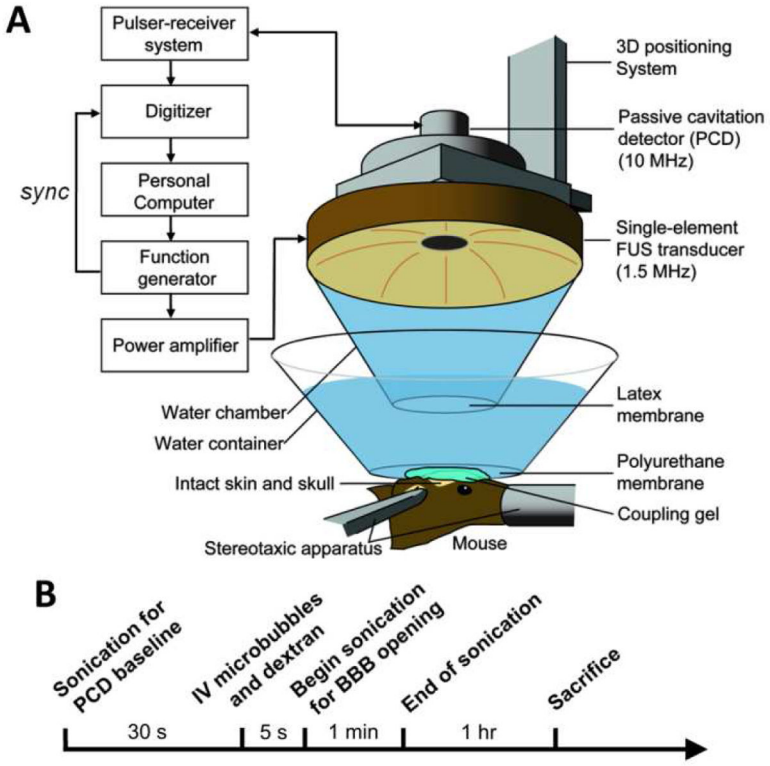

Fig. 2.

Experimental setup (A) and timeline (B) for FUS-induced BBB opening *in vivo*. A focused ultrasound (FUS) transducer in was used for sonication, while a pulse-echo transducer at the center of the FUS transducer was used to for both targeting and passive cavitation detection (PCD) purposes. After the targeting procedure, a 30 s of sonication before microbubble injection was performed as a baseline control for PCD. The freshly diluted microbubble solution was then co-administered with dextran intravenously, and the 1-min sonication for BBB opening started 5 s after injection. 1 hr after the end of sonication the mice was sacrificed using transcardial perfusion, and its brain was extracted and preserved for future processing.

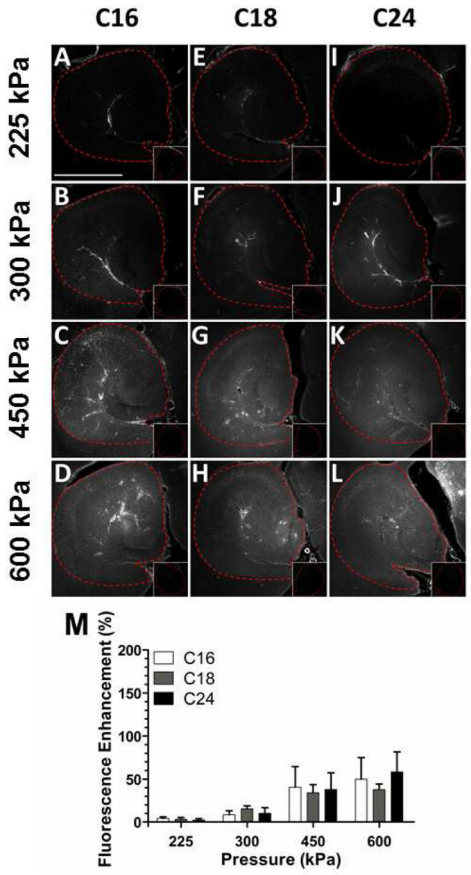

Fig. 3.

Effects of lipid hydrophobic chain length on delivery efficiency for 3-kDa dextran after FUS-induced BBB opening using 100-cycle (67 μs) pulses. (A–L) Representative fluorescence images comparing the targeted and the control (insets) hippocampi when C16, C18 or C24 microbubbles were used to mediate BBB opening at various pressures. The scale bar in A depicts 1 mm. (M) The quantified fluorescence enhancement between the sonicated and the control ROIs showed no significant shell effect on the 3-kDa dextran delivery across the BBB.

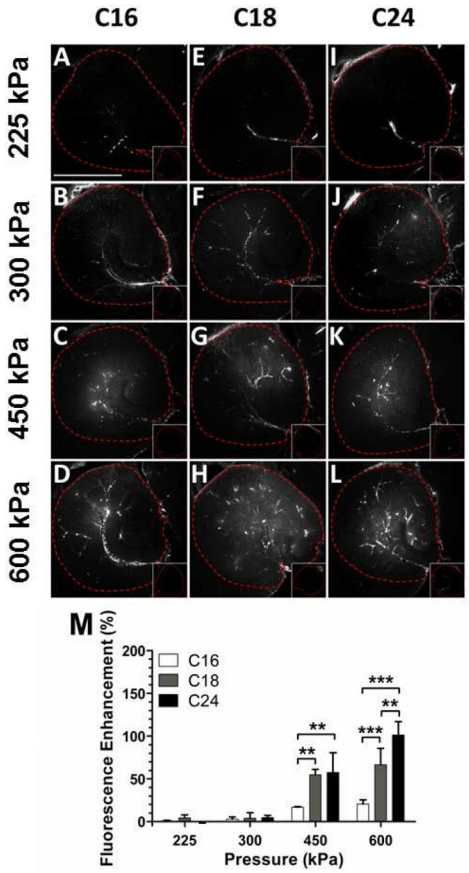

Fig. 4.

Effects of lipid hydrophobic chain length on delivery efficiency of 40-kDa dextran after FUS-induced BBB opening using 100-cycle (67 μs) pulses. (A–L) Representative fluorescence images compare the targeted and the control (insets) hippocampi when C16, C18 or C24 microbubbles were used to mediate BBB opening at various pressures. The scale bar in A depicts 1 mm. (M) The quantified fluorescence enhancement between the sonicated and the control ROIs showed significant shell effects on the 40-kDa dextran delivery across the BBB at higher pressures.

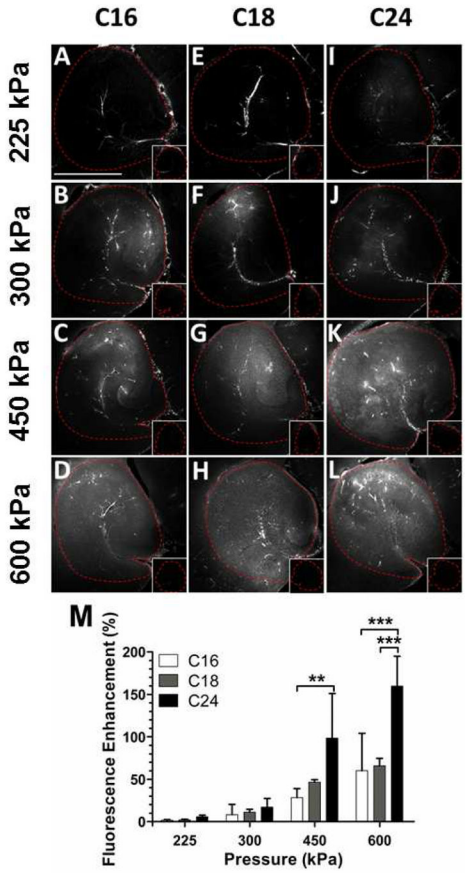

Fig. 5.

Effects of lipid hydrophobic chain length on delivery efficiency of 40-kDa dextran after FUS-induced BBB opening using 1000-cycle (670 μs) pulses. (A–L) Representative fluorescence images compare the targeted and the control (insets) hippocampi when C16, C18 or C24 microbubbles were used to mediate BBB opening at various pressures. The scale bar in A depicts 1 mm. (M) The quantified fluorescence enhancement between the sonicated and the control ROIs showed significant shell effects with C24 microbubbles on the 40-kDa dextran delivery across the BBB at higher pressures.

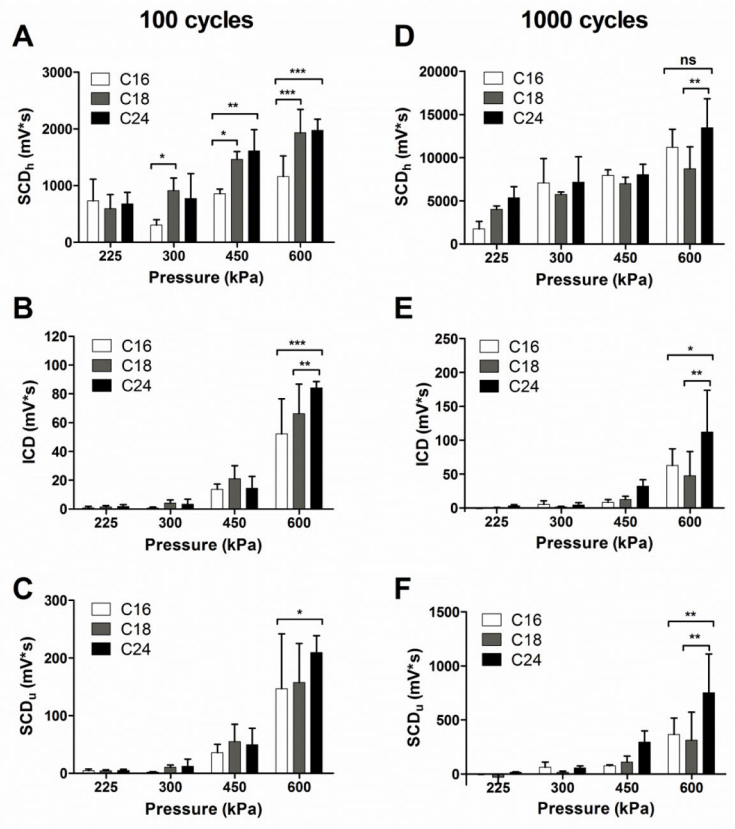

Fig. 6.

Quantified acoustic emission detected during BBB opening at various pressures and pulse lengths. For 100-cycle pulses, stable cavitation dose with harmonics (SCD_h) (A), inertial cavitation dose (B), and stable cavitation dose with ultraharmonics (SCD_u) (C) was calculated. The three types of cavitation dose for 1000-cycle pulses were also quantified (D–F).

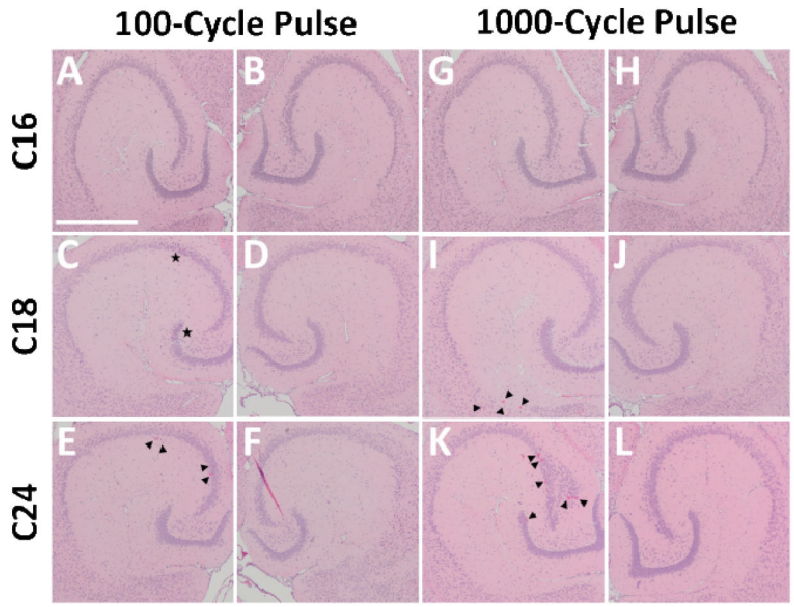

Fig. 7.

Representative histological images of the targeted (left) and control (right) hippocampi using 100-cycle (A–F) and 1000-cycle pulses (G–L) at 600 kPa. No erythrocyte extravasation, dark neurons, gross hemorrhage or microvacuolations were observed when C16 microbubbles were used to mediate BBB opening using either 100-cycle (A–B) or 1000-cycle (G–H) pulses. Small clusters of dark neurons (indicated with stars) were identified when C18 microbubbles were used with 100-cycle pulses (C–D), while a few petechial hemorrhages (indicated with triangles) were observed with 1000-cycle pulses (I–J). Larger degree of perivascular hemorrhages was seen with C24 microbubbles regardless of the pulse length (E–F, K–L). The scale bar in A depicts 1 mm.

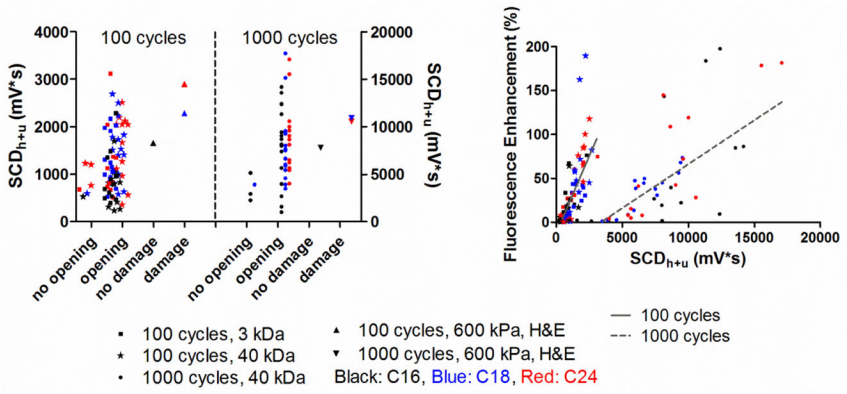

Fig. 8.

Using stable cavitation dose ($SCD_{h+u} = SCD_h + SCD_u$) to evaluate the opening outcomes qualitatively for classification (A) and quantitatively for delivery efficiency assessment (B). In the qualitative analysis (A), the SCD_{h+u} was separated into groups of no opening and opening (fluorescence enhancement was higher than the mean plus 2 times of standard deviation of the sham cohort), while based on the histological results it was separated into groups of no damage and damage (erythrocyte extravasation or dark neurons appeared). In the quantitative analysis (B), the fluorescence enhancement was positively correlated with the SCD_{h+u}, with a R^2 of 0.63 and 0.61 using linear fitting for 100-cycle pulses and 1000-cyle pulses, respectively.

Table 1

Summary of the experimental groups.

Group	Microbubble	Dextran (kDa)	Pulse Length (#Pulses)	Number of mice per experimental condition				
				Acoustic pressure (kPa)				
				Sham	225	300	450	600
1	DPPC (C16)	3	10^2	-	3	3	3	4[a]
	DSPC (C18)			-	3	3	3	4[a]
	DLiPC (C24)			-	3	3	3	4[a]
2	DPPC (C16)	40	10^2	-	3	3	3	3
	DSPC (C18)			-	3	3	4	3
	DLiPC (C24)			-	3	3	3	3
3	DPPC (C16)	40	10^3	-	3	3	3	4[a]
	DSPC (C18)			-	3	3	3	4[a]
	DLiPC (C24)			-	3	3	3	4[a]
4	-	3	-	5	-	-	-	-
5	-	40	-	3	-	-	-	-

[a]Number shown including 1 mouse per experimental condition used for histology examination.

Author Manuscript

Author Manuscript

Author Manuscript

Table 2

Microbubble physical properties[a]

Microbubble	Mean Diameter (μm)	Median Diameter (μm)	Mode Diameter (μm)
	Mean ± SD	Mean ± SD	Mean ± SD
DPPC (C16)	4.30 ± 0.20	4.25 ± 0.20	4.26 ± 0.21
DSPC (C18)	4.28 ± 0.15	4.26 ± 0.20	4.30 ± 0.16
DLiPC (C24)	4.20 ± 0.10	4.16 ± 0.16	4.24 ± 0.12

[a]Numbers shown here are from the number-weighted size distributions.